crystals

MDPI

Article

Comparison of Mechanical and Microstructural Properties of as-Cast Al-Cu-Mg-Ag Alloys: Room Temperature vs. High Temperature

Muhammad Farzik Ijaz, Mahmoud S. Soliman *, Ahmed Saad Alasmari, Adel Taha Abbas and Faraz Hussain Hashmi

Mechanical Engineering Department, College of Engineering, King Saud University, P.O. Box 800, Riyadh 11421, Saudi Arabia; mijaz@ksu.edu.sa (M.F.I.); 437105894@student.ksu.edu.sa (A.S.A.); aabbas@ksu.edu.sa (A.T.A.); 439106627@student.ksu.edu.sa (F.H.H.)

* Correspondence: solimanm@ksu.edu.sa

Abstract: Unfolding the structure–property linkages between the mechanical performance and microstructural characteristics could be an attractive pathway to develop new single- and polycrystalline Al-based alloys to achieve ambitious high strength and fuel economy goals. A lot of polycrystalline as-cast Al-Cu-Mg-Ag alloy systems fabricated by conventional casting techniques have been reported to date. However, no one has reported a comparison of mechanical and microstructural properties that simultaneously incorporates the effects of both alloy chemistry and mechanical testing environments for the as-cast Al-Cu-Mg-Ag alloy systems. This preliminary prospective paper presents the examined experimental results of two alloys (denoted Alloy 1 and Alloy 2), with constant Cu content of ~3 wt.%, Cu/Mg ratios of 12.60 and 6.30, and a constant Ag of 0.65 wt.%, and correlates the synergistic comparison of mechanical properties at room and elevated temperatures. According to experimental results, the effect of the precipitation state and the mechanical properties showed strong dependence on the composition and testing environments for peak-aged, heat-treated specimens. In the room-temperature mechanical testing scenario, the higher Cu/Mg ratio alloy with Mg content of 0.23 wt.% (Alloy 1) possessed higher ultimate tensile strength when compared to the low Cu/Mg ratio with Mg content of 0.47 wt.% (Alloy 2). From phase constitution analysis, it is inferred that the increase in strength for Alloy 1 under room-temperature tensile testing is mainly ascribable to the small grain size and fine and uniform distribution of θ precipitates, which provided a barrier to slip by deaccelerating the dislocation movement in the room-temperature environment. Meanwhile, Alloy 2 showed significantly less degradation of mechanical strength under high-temperature tensile testing. Indeed, in most cases, low Cu/Mg ratios had a strong influence on the copious precipitation of thermally stable omega phase, which is known to be a major strengthening phase at elevated temperatures in the Al-Cu-Mg-Ag alloying system. Consequently, it is rationally suggested that in the high-temperature testing scenario, the improvement in mechanical and/or thermal stability in the case of the Alloy 2 specimen was mainly due to its compositional design.

Keywords: as-cast; Al-Cu-Mg-Ag alloy; Cu/Mg ratio; peak aged; tensile test; mechanical properties

Citation: Ijaz, M.F.; Soliman, M.S.; Alasmari, A.S.; Abbas, A.T.; Hashmi, F.H. Comparison of Mechanical and Microstructural Properties of as-Cast Al-Cu-Mg-Ag Alloys: Room Temperature vs. High Temperature. *Crystals* **2021**, *11*, 1330. https://doi.org/10.3390/cryst11111330

Academic Editors: Alexander S. Novikov and Assem Barakat

Received: 21 September 2021
Accepted: 28 October 2021
Published: 31 October 2021

1. Introduction

Single-crystal and polycrystalline aluminum (Al) alloys have garnered considerable interest in the automotive and aviation industries owing to their alluring properties, such as being lightweight, high formability, and corrosion resistance [1–6]. Indeed, further insight into the structure–performance relationship of the established polycrystalline system may allow researchers to extrapolate experimental findings to other similar types of single-crystalline systems that could be developed for specific applications [7–10]. It is worth stressing that, the density of iron (Fe) is approximately 7.8 g/cm^3, which is more than 2.8 times higher than that for Aluminum (Al), which makes Al and its alloys promisingly

versatile for several applications, particularly where cost saving and the benefits of the fuel economy are essential [11]. Despite the appealing combinations, the as-cast and wrought Al alloys still only have half of the mechanical properties of steel that are needed to carefully account for future advanced applications. In addition, with the improvement in mechanical properties such as strength, there is a ductility trade-off for high-temperature applications in the temperature range of 150–300 °C, which are the average temperatures that are normally attained in automotive engine components under actual in-service conditions, which also remains a significant challenge that needs to be resolved. [1,3,5,12].

For instance, to date, various cast and wrought aluminum 2xxx (Al-Cu or Al-Cu-Mg) alloys have been fairly well investigated with numerous alloy design concepts and/or through the addition of suitable alloying elements. In this context, the important alloying elements used to improve the mechanical properties of pure aluminum (Al) are mainly silicon (Si), magnesium (Mg), manganese (Mn), copper (Cu), and zinc (Zn) [13–16]. Nevertheless, the addition of Cu as a principal alloying element with Mg as the ternary alloying element has also been increasingly studied over the years because the simultaneous addition of Cu and Mg to parent aluminum Al has two major advantages. Firstly, the cumulative effects of Cu and Mg improve the mechanical properties, including the hardness and ultimate tensile strength of the pure α–Al matrix through a classical solid solution strengthening effect. Secondly, through low-temperature annealing and/or aging treatment, the Cu and Mg solute elements can effectively elicit the precipitation of primary intermetallic compounds. Likewise, with respect to compositional design of the Al–Cu–Mg alloy with a low Cu to Mg ratio (e.g., Al 2024), precipitation behavior is mainly dominated by the formation of a magnesium-rich phase [Al_2CuMg (S-precipitate)], which has an orthorhombic structure lying on a {210} Al habit plane [6]. In comparison, a high Cu to Mg ratio stimulates the formation of copper-rich phases of [Al_2Cu (θ′-precipitate)] which lie on the {001} Al habit plane [16–20], such as copper-rich phase (Al_2Cu, θ) and (Al_2CuMg, *S*) from the supersaturated solid solution of α–Al matrix. The overall dispersion strengthening mechanism by the virtue of these precipitates in this kind of alloy depends upon various factors, such as size, shape, spatial distribution, and volume fraction of the different intermetallic phases. The kinetic and precipitation development mechanisms and their influence on mechanical properties in the Al-Cu-Mg alloying system have been widely reported in the literature [21–24]. For example, it is widely believed that the ternary addition of silver (Ag) to Al-Cu-Mg-based alloys promotes the formation of an Mg-Ag co-cluster, which acts as a precursor for the nucleation of well-known Ω-phase precipitates during aging treatment. The formation of secondary Ω-phase precipitates along with primary phases can remarkably increase the strength of the α–Al matrix by precluding the dislocation motion on slip planes in the fcc cell of the α–Al matrix [25,26]. To date, different precipitation kinetic models and mechanisms for the formation of the Ω phase have been proposed, which are often linked with the chemical composition of the alloying system, i.e., Cu/Mg ratios, but without a full understanding of the processes and chemical composition linked to the unique Ω phase, these are not conclusive [25–27]. Nevertheless, the influence of the Ω phase on the high-temperature thermal and mechanical properties of Al-Cu-Mg-based alloys cannot be neglected [28,29].

Thus, from the viewpoint of ensuring the economical and lightweight manufacturing of complicated structural parts like cylinder blocks, transmission cases, and converter housings, the as-cast aluminum alloy should be given preference. It should be noted that the as-cast alloys are directly formed into the desired shape by casting appropriate dimensions without any further machining/plastic deformation. During solidification, intermetallic compounds are formed that affect the mechanical properties, inevitably leading to a decrease in ductility compared with to its wrought alloy counterpart. This is because the intermetallic compound could act as a potential crack initiation site [1,3,29]. Furthermore, at a high temperature above 200 °C, this issue is further exacerbated for the heat-treatable cast aluminum alloys. Indeed, the intermetallic compound grows more rapidly due to the difference in the diffusion rate of elements, resulting in marked degradation of the

mechanical properties. Consequently, the main challenge still lies in finding the best balance between ductility at room temperature and strength at higher temperature for as-cast Al-based alloys [30]. Nonetheless, the strength of Al-based alloys decreases drastically at temperatures above 200 °C, therefore special considerations must be given to ensure microstructural integrity for long-term high-temperature applications. Ultimately, this understanding can then be useful to design single-crystalline Al alloys that have more optimal combinations of properties across a wide range of processing conditions.

To date, several studies have been done to design Al-Cu-Mg-based alloys and then investigate the effect of micro-alloying on the precipitation scenario and the resulting mechanical properties. Thus, different processing parameters, including solution treatments and aging processes, can also significantly modify the microchemistry and can generate various textures in the alloys. In this context, temperature-dependent diffusion and the grain growth, attributable to the solute element, like Mg, revealing the static recrystallization texture in Al-based alloys, are also well known [31–33]. Nonetheless, heat treatment conditions could also be an additional factor that should be considered in tuning the excellent mechanical properties. For example, Wang et al. [33,34] have discussed that besides the precipitation scenario, the textures also play a distinct role in the mechanical performance.

To date, although there has been widespread literature covering important data on the characteristics of as-cast Al-Cu-Mg-based alloys that can aid in design and analysis of this kind of alloy, quite recently, it has been found that the doping of yttrium in the Al-Cu-Mg-Ag alloy could be detrimental to the mechanical performance of the T6 tempered Al-Cu-Mg-Ag alloy at room temperature but enhance the strength properties at 300 °C due to the formation of Al_8Cu_4Y intermetallic [35]. Likewise, Xie et al. [36] also provided the same conclusion for the effect of rare earth elements, in their case, an erbium (Er) addition was made to an as-cast Al-Cu-Mg-Ag alloy, from which they suggested that the strength properties of Er-added alloys at 300 °C were found to be enhanced, benefitting from the pinning effect of the Al_8Cu_4Er phase on grain boundaries. Meanwhile, the detrimental effect of undissolved second phases and/or impurities at the grain boundaries could also have an adverse effect on the mechanical properties [36–40]. This is because the brittle phase could result in undesirable rapid crack growth during mechanical testing. Encouragingly, Zamani et al. [40], in the quest for improved properties, discussed the optimization of heat treatment parameters, i.e., artificial aging temperatures on the hardness values for as-cast Al-Cu-(Mg-Ag) alloys. They claimed that the addition of Mg to Al–Cu alloys promoted the formation of phases with a rather low melting temperature, which demand multi-step solution treatment. While the presence of Ag decreases the melting temperature of intermetallic (beside Al_2Cu), it improves the age-hardening response [40]. Yet, their work focused only on the experimental results about hardness values, and the experimental results encompassing mechanical properties, like ultimate tensile strength, were not performed.

Surprisingly, to the best of our knowledge, there have been very few comprehensive studies that correlated the effects of alloying elements on room- and high-temperature tensile properties of as-cast Al-Cu-Mg-Ag alloys with different Cu/Mg ratios. Therefore, the room-temperature and elevated-temperature mechanical properties required to analyze the structural response of polycrystalline aluminum alloys of interest must be evaluated and compared in regards to compositional design and scenarios. The present work was mainly designed to fill this gap. The key point in this research was to find out the potential of as-cast alloys for light-weight structures. We discuss the performance of two different alloys with distinct Cu/Mg ratios at room and high temperatures. Finally, perspectives on alloy compositional design and our experimental strategy, emerging microstructural evolution results are discussed. This work provides a preliminary thorough analysis of the current status of polycrystalline Al-Cu-Mg-Ag alloys and highlights important avenues for future work.

2. Materials and Methods

The two alloys with nominal compositions were designed depending upon the high and low Cu/Mg ratio. The nominal compositions were Al-2.89Cu-0.23Mg-0.65Ag (wt.%) (hereafter referred to as Alloy 1: Cu/Mg = 12.6) and Al-2.96Cu-0.47Mg-0.65Ag (wt.%) (hereafter referred to as Alloy 2: Cu/Mg = 6.3). The designed alloys (i.e., Alloy 1 and Alloy 2) were prepared by melting the high-purity commercial raw materials, like pure Al (99.97%), Cu (99.9%), Ag (99.9%), and Al-20% Mg master alloy, by utilizing the medium-frequency induction furnace. After thorough melting in the graphite crucible at 720 °C, the alloys were cast in a heated steel permanent mold (450 °C) to produce rods with dimensions of 85 mm in length and 15 mm in diameter. The preheated mold and mechanical stirring were performed to mitigate the conventional casting-associated defects. Both Alloy 1 and Alloy 2 underwent similar casting procedures. Following the casting step, the as-cast rods of both the alloys were homogenized in an air furnace at 520 °C for 24 h. The compositions of the as-cast alloys, i.e., Alloy 1 and Alloy 2, were then determined by using arc and spark excitation metal analyzer Spectromax from Spectra Company. An overview of the investigated alloys with their actual compositions and Cu/Mg ratios are listed in Table 1. All the compositions hereinafter are actual and in wt.% unless otherwise specified.

Table 1. The chemical composition of the experimental alloys.

Alloys	Cu/Mg	Chemical Composition (wt.%)			
		Cu	Mg	Ag	Al
Alloy 1	12.6	2.89	0.23	0.65	Balance
Alloy 2	6.3	2.96	0.47	0.65	Balance

Following the homogenization steps, the as-cast Alloy 1 and Alloy 2 specimens were solid-solution-treated (SST) at 520 °C for 8 h and then quenched in water to create a supersaturated solution of α phase at room temperature. Following solution treatment, the aging heat treatment was performed. The aging treatments were carried out in a constant temperature drying oven (CARBOLITE furnace); both Alloy 1 and Alloy 2 were aged in a salt bath mixture consisting of 50% potassium nitrate, KNO_3 (Lobachemic) and 50% sodium nitrite, $NaNO_2$ (Pharma). The mixture was placed into a graphite crucible and heated in the furnace for 5 h before the aging process started at 190 °C, which was measured by a thermocouple immersed in the salt bath. Samples were also quenched with water after each aging condition.

To establish the effect of composition and to evaluate the peak hardening condition, hardness testing was performed after the artificial aging treatment process. The average Vickers hardness number (VHN) of each of the Alloy 1 and Alloy 2 specimens, aged for different lengths of time, was calculated from five indents using a Vickers hardness tester (WOLPERT UH930, Wilson Hardness, Shanghai, China). Each indentation was performed by imposing a load of 10 kg for 15 s.

To observe the microstructural features, such as the average grain size, the optical microscopy observation was made for the as-cast, solution-treated, and peak-aged state of both alloys. The surface of the specimens for optical observation was prepared by grinding from 500 to 1200 grit and mirror polishing while using 0.05 μm alumina particles. The etching of the specimens was performed per ASTM E 407-99 standard (2 mL HF, 3 mL HCl, 5 mL HNO_3, and 200 mL H_2O). The etching was used not only to delineate grain boundaries but also to allow the different phases to appear by differences in brightness, shape, and color. After etching, the optical microstructures were observed with an optical microscope (Olympus BX51M, Tokyo, Japan).

Furthermore, the phase constitutions in the solution-treated (sol. treated) and peak-aged (PA) treatment were investigated at room temperature using the X-ray diffractometer (model: D-8 Discover, Bruker, Berlin, Germany) machine with CuK_α monochromatic X-ray radiation and a tube current of 15 mA and voltage of 30 kV.

Finally, to distinguish the effect of the composition (i.e., Mg content) on the mechanical properties, tensile testing was carried out in two distinct environments i.e., room-temperature (RT = 25 °C) and high-temperature (HT = 180 °C). Specimens for tensile test samples were machined from the solution-treated rods and went through a peak aging treatment, as discussed above. The tensile samples were designed according to the famous ASTM E8 standard. The cylindrical tensile specimens had gage length (Lo)/gage diameter (Do) = 4. A comparison of mean mechanical properties, particularly ultimate tensile stress (σ_{UTS}), was made between two sample sets for each scenario of testing. For this research, the only tensile test results needed for analysis were changes in ultimate strengths across the environments used. Therefore, owing to the small specimen size and harsh elevated temperature environment, the extensometer was not used during tensile testing for any scenario of tensile testing (both RT and HT) and the strain was calculated simply by using crosshead displacement alone. It is believed that this machine compliance adjustment had a negligible effect on data acquisition for this research. The tensile properties at room and elevated temperatures were investigated by using an Instron universal electronic testing machine model 3385H, with a data acquisition system, at a constant speed of 1 mm/min corresponding to an initial strain rate of 6.7×10^{-4} s^{-1}. Finally, engineering stress–strain curves were plotted and were not corrected for machine compliance.

3. Results and Discussion

3.1. Effect of Cu/Mg Ratio on the As-Cast Microstructure

Figures 1 and 2 show the phase constituent and microstructural analyses of the as-cast state of Alloy 1 (high Cu/Mg ratio) and Alloy 2 (low Cu/Mg ratio), respectively. Figure 1 shows the diffraction pattern plots of intensity against the angle of the detector, 2θ at room temperature. As shown in Figure 1 the XRD profile of both studied alloys displayed the strong characteristic peak of α-Al and very small peaks of precipitates [18,40–44], which have been marked by black arrows in Figure 1. Similarly, Figure 2 shows the optical microscopy results; broadly, the microscopic observations were consistent with the XRD analysis. From the optical microscopy observation, the main phase of both Alloy 1 (high Cu/Mg ratio) and Alloy 2 (low Cu/Mg ratio) was the α-Al (parent phase), with a moderate volume of black-colored precipitates of θ-Al_2Cu [14]. It is believed that θ-Al2Cu, with different sizes and varying aspect ratios (as marked with arrow in Figure 2), was formed during the air-cooling stage of the casting. In general, the as-cast structures of both Alloy 1 (high Cu/Mg ratio) and Alloy 2 (low Cu/Mg ratio) were predominated by a great number of equiaxed grains with average grain size of 60 μm. It can be assumed that the difference in Cu/Mg ratio revealed a negligible change in grain size and morphological and microstructural characteristics of Alloy 1 and Alloy 2 after the casting and solidification steps. Figures 1 and 2 show the phase constituent and microstructural analyses of the as-cast state of Alloy 1 (high Cu/Mg ratio) and Alloy 2 (low Cu/Mg ratio), respectively.

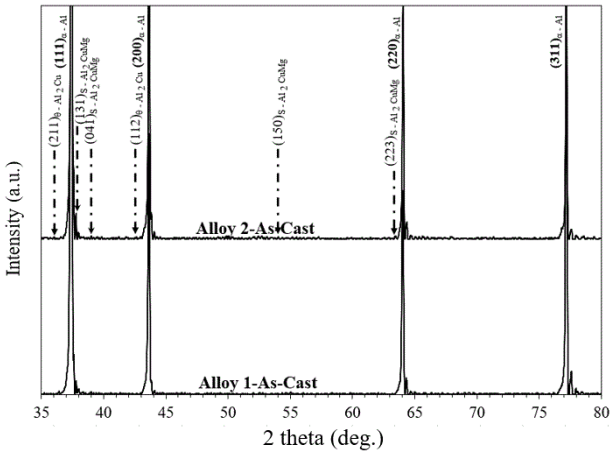

Figure 1. X-ray diffraction patterns of the as-cast state Al-Cu-Mg-Ag alloys.

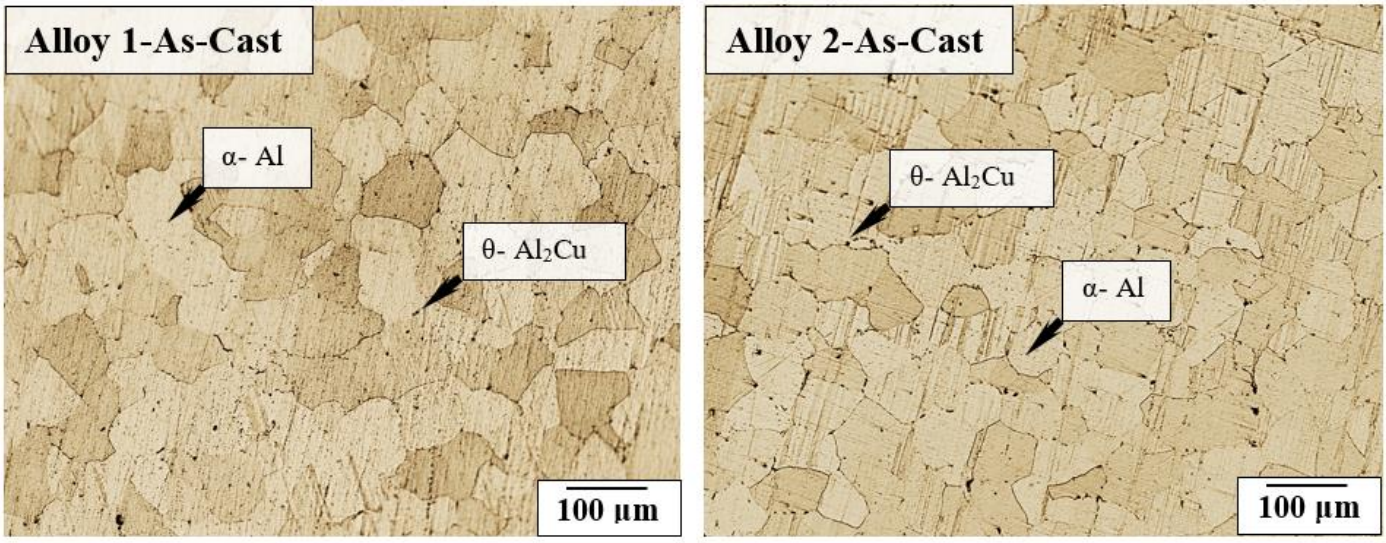

Figure 2. Cross-sectional optical microscopy (OM) observations of the as-cast state of the Al-Cu-Mg-Ag alloys, showing mainly the α-Al (matrix) and black-colored θ-Al_2Cu (precipitates).

3.2. Effect of Cu/Mg Ratio on Phase Constitution of As-Cast Solution-Treated Alloys

Figure 3 shows the diffraction pattern plots of intensity against the angle of the detector, 2θ at room temperature. The X-ray diffraction (XRD) profiles of Alloy 1 and Alloy 2 after the solution heat treatment at 520 °C for 8 h reveal the strong characteristic peaks of the α-Al phase. However, the XRD profile of both the specimens after solution heat treatment indicates additional peaks along with the α-Al phase. These additional peaks could easily be identified as the Al_2Cu phase and Al_2CuMg precipitates [42,43]. These precipitates were the product of several constituent phases (implying they formed as solidification products and survived the homogenization treatment). Similar results have also been demonstrated in an as-cast Al-Cu-Mg-Ag alloy [36,37,44].

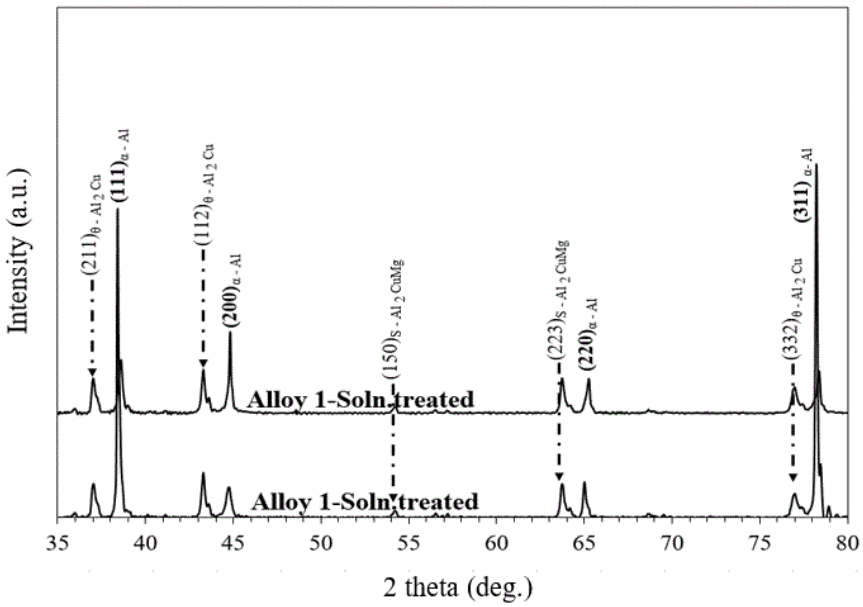

Figure 3. X-ray diffraction patterns of the solution-treated (Sol. treated) Al-Cu-Mg-Ag alloys.

Figure 4 shows the optical microstructure of the Alloy 1 and Alloy 2 at the peak-aged state. It should be noted that these solute-rich precipitates were coarser in the specimen containing higher Mg-content (Alloy 2). From the XRD results shown in Figure 3, these solute-rich precipitates (second phase) were Al_2Cu and Al_2CuMg precipitates. Further-

more, it can be observed that for Alloy 1, the overall grains were mostly equiaxed, with an average grain size of approximately 62 µm. On the other hand, the Alloy 2 specimen at solution treated state revealed an abnormal grain growth with an average grain size of 412 µm.

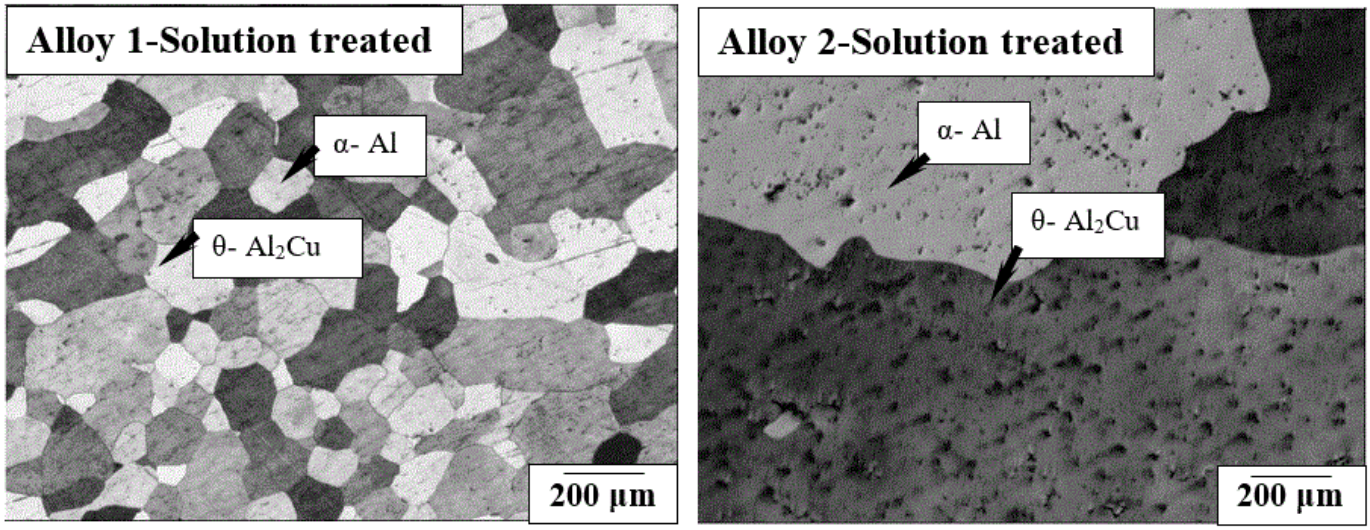

Figure 4. Cross-sectional optical microscopy (OM) observations of the solution-treated (Sol. treated) Al-Cu-Mg-Ag alloys showing mainly the α-Al (matrix) and black-colored θ-Al_2Cu (precipitates).

3.3. Effect of Cu/Mg Ratio on the Age-Hardening Behavior

To understand the age-hardening behavior of the studied alloy, Vicker hardness testing was performed on as-cast Alloy 1 and Alloy 2 after the aging treatment. Figure 5 shows the age-hardening curve of as-cast Alloy 1 and Alloy 2, respectively, after the artificial aging process at 190 °C for varying times. The age-hardening curve was obtained after the completion of three heat treatment steps—solution annealing, quenching, and aging.

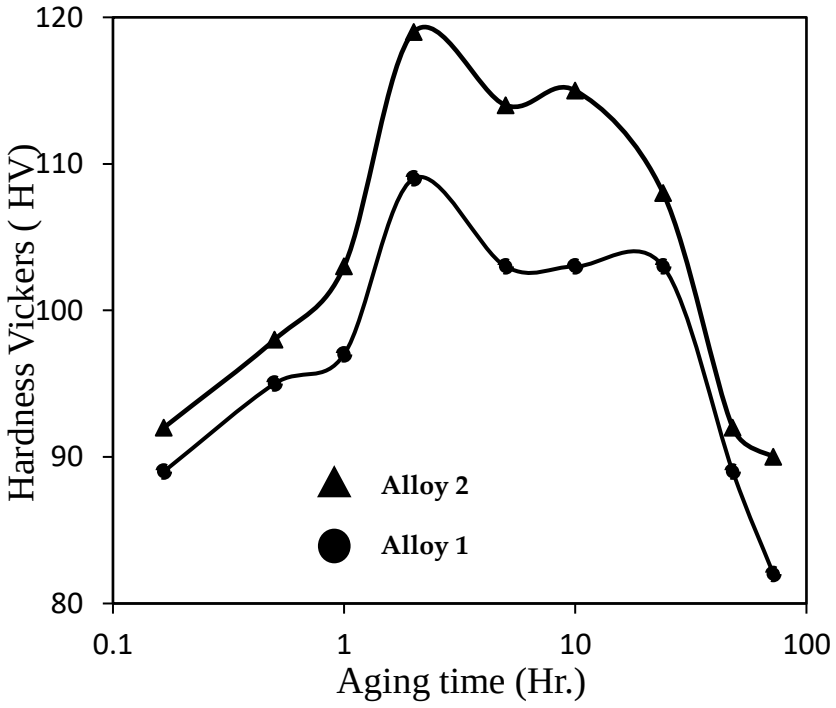

Figure 5. Aging curves of as-cast Alloy 1 and Alloy 2, showing HV10 vs. aging time after the ageing heat-treatment process.

Figure 5 summarizes the entire age-hardening behavior of Alloy 1 and Alloy 2. When comparing both alloys, it is obvious that the Alloy 2 revealed a slightly higher hardness value in the solution-treated state, i.e., at 0 h, when compared to Alloy 1, this increase in hardness value could be attributed to the well-known chemical composition effect, i.e., high Mg content. Owing to the difference in the atomic size of the alloying element and the higher amount of solute content, it is plausible that higher hardness could be attributed to local lattice distortion, which would have raised the energy barrier against dislocation movement during the indentation, giving rise to the solid solution phenomenon. Moving further, it is evident that from the beginning of the artificial aging process there was a progressive increase in hardness values for both of the alloys, which is consistent with the previously reported literature [13,17,18,30]. The monotonic increase in hardness values can be related to the formation of precipitation phases from the supersaturated Al matrix. In general, the hardening tendency increased with an increase in aging time, reaching a maximum value (peak-aged state—PA), and then progressively decreased with further aging, leading to an overaged point (T7). The sharp softening occurred because of matrix recovery and overaging effects; the overaging effect was more remarkable in Alloy 1, mainly due to less formation of coarsening-resistant precipitates of the omega phase [20,21].

The peak aging times for Alloy 1 and Alloy 2 were almost the same and could be attributed to 2 h. Indeed, the average value of hardness at the peak aging time was around 119 HV at 2 h for Alloy 2 and 109 HV for Alloy 1 after about 2 h, as shown in Figure 2. The slightly higher value of hardness at the peak aging time in the Alloy 2 specimen when compared to the Alloy 1 specimen could be related to the Mg level (solid solution strengthening effect) and the Cu/Mg ratio [13,15,44].

3.4. Effect of Cu/Mg Ratio on Phase Constitution of Peak-Aged Alloys

Figure 6 shows the XRD profiles corresponding to the peak-aged state of both alloys. The phase constitution was changed by a change in Cu/Mg ratio. For the alloy containing a higher Cu/Mg ratio (Alloy-1), as seen in Figure 6, the peaks corresponding to the α-Al phase revealed significantly higher intensity when compared to the alloy containing a low Cu/Mg ratio. The relative changes in intensity of the diffraction peaks were most likely due to the formation of static recrystallization texture. The formation of preferred static recrystallization during aging treatment by the virtue of a solute element, in our case Mg, has also been reported in previous studies [45–47]. It is also clear, by comparing the XRD profiles of Alloy 1 and Alloy 2, that the change in Cu/Mg ratio altered the precipitation scenario. Thus, from the XRD profiles, besides the matrix phase (Al), the additional peaks corresponding to the precipitation phases were also detected for both Alloy 1 and Alloy 2, respectively (as shown in Figure 6). These additional peaks could be indexed as Al_2Cu (θ) phase (tetragonal structure, 14/mcm, a = 0.6066 nm, c = 0.4878 nm) and Al_2CuMg (S) phase (orthorhombic structure, Cmcm, a = 0.400 nm, b = 0.923 nm, c = 0.580 nm) [37,41–44]. The Al_2Cu (θ) phase and Al_2CuMg (S) phase co-existed in both the high- and low-Cu/Mg-ratio compositional scenarios. However, it is noteworthy that the peaks from the θ phase were greater in the high-Cu/Mg alloy when compared to the low-Cu/Mg alloy, which is also consistent with previous literature. Indeed, a higher Cu/Mg ratio in Al-Cu-Mg-Ag alloys promotes the formation of the θ phase, whereas the development of favorable recrystallization during aging treatment is believed to be a result of solute segregation in response to a planner defect, such as grain boundaries. To complement this assumption, grain sizes of both the alloys were observed and will be discussed in the next section.

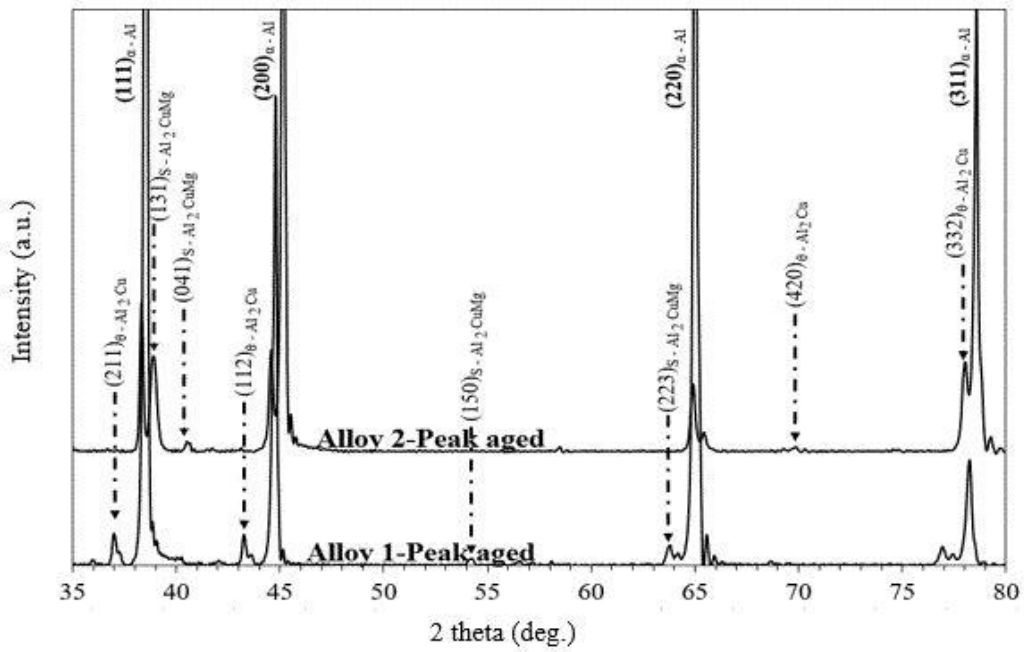

Figure 6. X-ray diffraction patterns of the peak-aged treated (PA) Al-Cu-Mg-Ag alloys.

3.5. Effect of Cu/Mg Ratio on the Microstructure Evolution of Peak Aged Alloys

Figure 7 shows the optical microstructure of Alloy 1 and Alloy 2 at the peak-aged state. It should be noted that these solute-rich precipitates were coarser in the specimen that contained higher Mg content (Alloy 2). From the XRD results, as shown in Figure 6, these solute-rich precipitates (second phase) on the microscopic images were Al_2Cu and Al_2CuMg precipitates which is consistent with XRD results. Furthermore, it was observed that for Alloy 1, the overall grains were mostly equiaxed, with an average grain size of approximately 62 μm. On the other hand, the Alloy 2 specimen at peak-aged state revealed an abnormal grain growth with a grain average size of 412 μm. From the viewpoint of abnormal grain growth, as observed in the case of Alloy 2, the predominant role of the solute element (Mg content) and small volume fraction of the pinning particle and/or precipitates causing this abnormal grain growth could not be neglected [44–46]. The lesser pinning force exerted by precipitate particles of a second phase on the grain boundary in the case of Alloy 2 when compared to Alloy 1 could be an important factor for this surprising microstructural evaluation and abnormal grain growth. From our current understanding, it is suggested that, owing to less boundary pinning induced by the solute and/or Zener drag by the second-phase particle formation, after the aging treatment process, especially for the Alloy 2, the grains with a topological advantage would possess sufficient boundary velocities to overcome solute drag and grow rapidly relative to other grains [47,48]. This microstructure and texture evolution have led to the occurrence of abnormal grain growth [49]. Although detailed investigation for the driving mechanism of grain growth and the resulting recrystallization texture is very interesting, it falls beyond the scope of the present study. The abnormal grain growth phenomenon owing to solute elements has been widely discussed in the past in many metallic materials, e.g., magnesium alloys, stainless steels, Fe-Si steel, titanium alloys, and aluminum alloys [50–55].

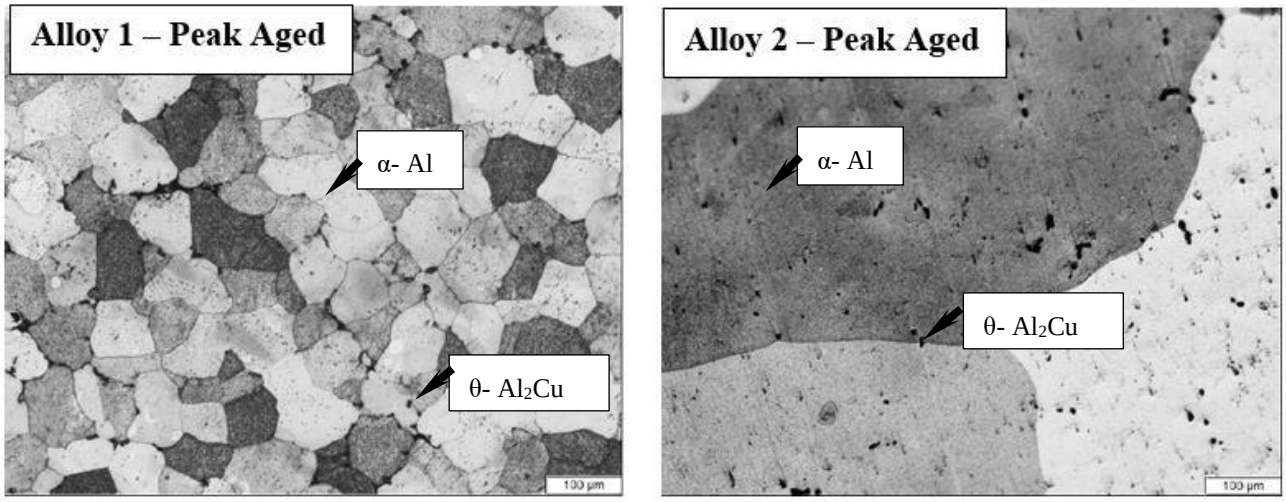

Figure 7. Cross-sectional optical microscopy (OM) observations of the peak-aged treated (PA) Al-Cu-Mg-Ag alloys.

3.6. Effect of Cu/Mg Ratio on the Room-Temperature Mechanical Properties of Peak-Aged Alloys

Figure 8 displays the tensile properties of Alloy 1 and Alloy 2 at the peak-aged state. Mechanical properties were evaluated by the tensile test, which was done by pulling the specimen until fracture. From Figure 8, it is clearly illustrated that tensile properties, especially the ultimate tensile strength, typically improved when the Cu/Mg ratio was increased from 6.30 to 12.60. In the room-temperature mechanical testing scenario, the higher Cu/Mg ratio alloy, with Mg content of 0.23 wt.% (Alloy 1), possessed higher ultimate tensile strength when compared to the low Cu/Mg ratio, with Mg content of 0.47 wt.% (Alloy 2). The increase in strength of Alloy 1 when compared to Alloy 2 at room temperature (RT) can be explained via two aspects. The first one is on the basis of the grain boundary strengthening phenomenon, since Alloy 1 had an appreciably smaller grain size when compared to Alloy 2 (as shown in Figure 7). Therefore, on the theory of the Hall–Petch coefficient (k), it is reasonable to claim that the resistance to dislocation slip in Alloy 1 was higher when compared to Alloy 2. Secondly, the precipitation strengthening elicited from the θ and S precipitates also needs to be taken into account in the improvement of mechanical strength at room temperature. Nonetheless, in the room-temperature tensile testing environment, the effect of grain refinement strengthening was far greater than the precipitation strengthening. [13,15,18,20,27,31,42].

3.7. Effect of Cu/Mg Ratio on the High-Temperature Mechanical Properties of Peak-Aged Alloys

Figure 9 displays the high-temperature tensile properties of Alloy 1 and Alloy 2 in the peak-aged state. The summary of the tensile properties showing the comparison of room-temperature vs. high-temperature tensile testing is also listed in Table 2. Alloy 2, with low Cu/Mg ratio, exhibited less degradation in the mechanical properties when compared to Alloy 1. Indeed, Alloy 2 showed a relatively higher value of ultimate tensile strength, which was above 200 MPa. It is well known that the improvement in the thermal stability at elevated temperature is plausible from the formation of high coarsening resistance of the omega phase (Ω) plate formation, but our experimental results make the relationships more explicit, which is inconsistent with previous studies [13–18,20–24]. Interestingly, from the viewpoint of omega phase formation (Ω), it is noteworthy that although Ag content was the same in both Alloy 1 and Alloy 2, it is strongly believed that the presence of Mg atoms together with Ag atoms greatly stabilizes the interface structure and, consequently, promotes the Ω phase on the Al {1 1 1} habit planes. Hence, mechanical properties at elevated temperatures were mainly improvised by the alloying elemental chemistry, i.e., higher Mg atoms. In other words, it is plausible, in our case, that the higher content of Mg atoms in Alloy 2 has provided the additional driving force of the precipitation of a nano-scaled Ω phase under stress, which has resulted in an improvement in the mechanical

results at elevated temperatures (especially σ_{UTS}) of Alloy 2 when compared Alloy 1. Similar sensitivity of mechanical properties to microstructural variability development has also been observed in Al–Cu–Mg alloys [56]. Having said that, indeed, this assumption needs some further research and it will be taken in account in our future works. Owing to severe high-temperature-related challenges, the realization of systematic in situ nano-scaled precipitation evidence of the omega phase and additional co-precipitation phases is not presented in this study and might be supported in the future by in situ TEM/XRD characterizations. In conclusion, the improvement in thermal stability of Alloy 2 could be strongly influenced by the alloy chemistry attributed from its unique compositional design. Less degradation in the mechanical properties at high temperatures could be due to matrix strengthening [57]. In conclusion, the high-temperature behavior of as-cast Alloy 2 was found to be not similar to the conventional general wrought ductile alloys.

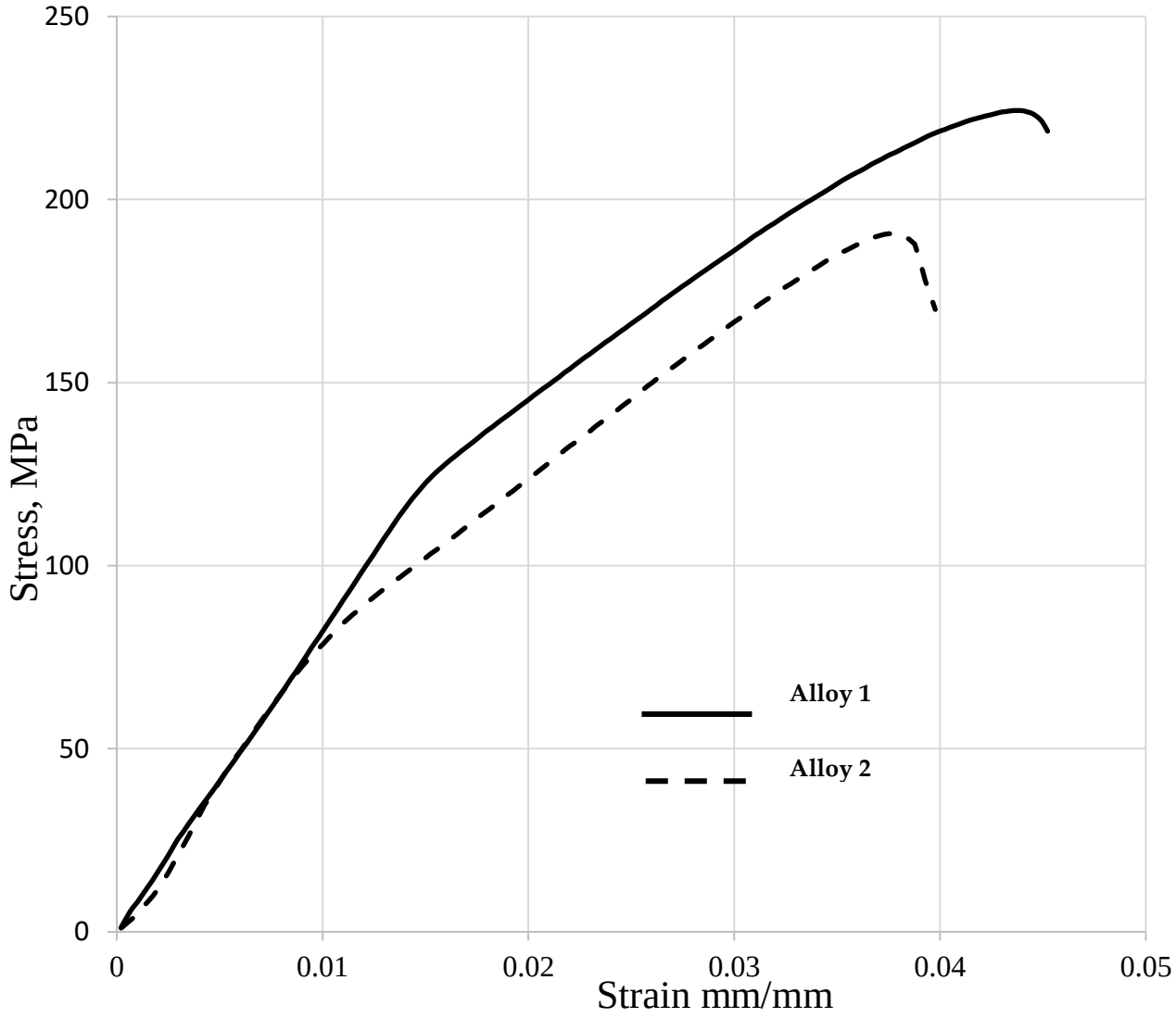

Figure 8. Engineering stress vs. strain curves of the peak-age-treated (PA) Al-Cu-Mg-Ag alloys at room temperature.

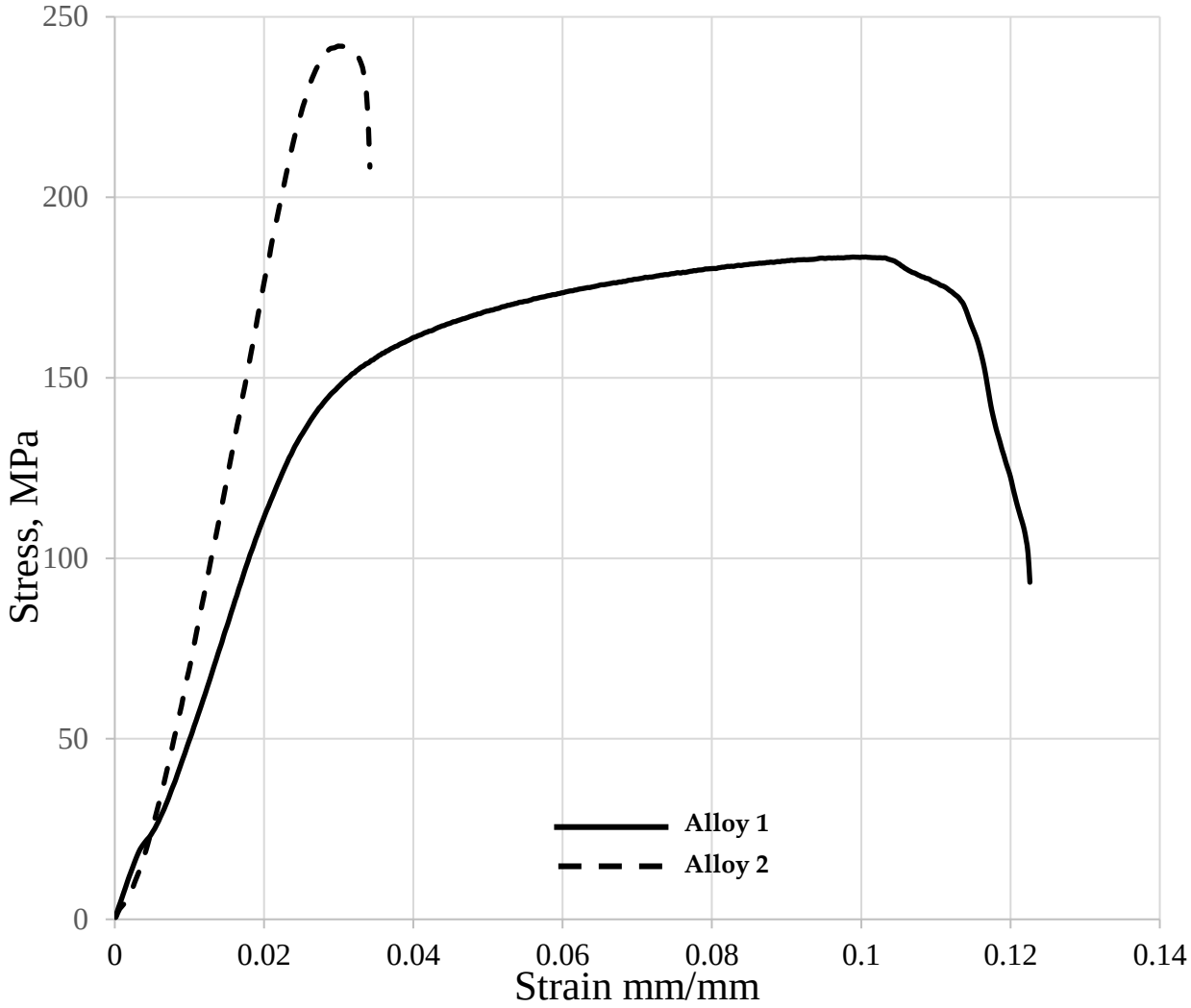

Figure 9. Engineering stress vs. strain curves of the peak-age-treated (PA) Al-Cu-Mg-Ag alloys at 180 °C.

Table 2. Comparison showing the difference of mechanical properties with respect to the testing environment.

Mechanical Properties/Environment	Alloy 1	Alloy 2
UTS—[180 °C]	183	242
UTS—[RT]	224	190
Elongation to Fracture (e_f %) [RT]	4.5	3.9
Elongation to Fracture (e_f %) [180 °C]	12.2	3.4

4. Conclusions

The effects of Cu/Mg ratio and peak-aging heat treatments on the microstructure, hardness, and aging kinetics of the as-cast Al-Cu-Mg-Ag alloys were investigated. The following conclusions are summarized:

- From XRD profiles, it was found that the Al_2Cu phase was more denominated in the higher Cu/Mg ratio alloy (Alloy 1) when compared to the lower Cu/Mg ratio alloy (Alloy 2).
- The peak intensity of Alloy 2 after ageing treatment showed stronger intensity and larger grain size, which is attributed to lower pinning pressure of the second phase particles.
- The mechanical properties were evidently sensitive to the testing environment and possible microstructure developments, which was manifested in high tensile strength of Alloy 2 at 180 °C.

- Increasing the Cu/Mg ratio was advantageous to the mechanical properties at room temperature for the peak-aged specimens but decreased the mechanical strength properties at 180 °C. The high Cu/Mg ratio alloy had an ultimate tensile strength of 224 MPa at room temperature, which decreased to 183 MPa at 180 °C.

Author Contributions: Writing-original draft, Methodology, Conceptualization, Writing –review & editing, M.F.I.; Resources, Investigation, Funding Acquisition, Writing-review & editing, M.S.S.; Data curation, Investigation, A.S.A.; Supervision, Visualization, A.T.A.; Data curation, Formal Analysis, F.H.H. All authors have read and agreed to the published version of the manuscript.

Funding: This work was funded by Research Center, College of Engineering, King Saud University and also support from Deanship of Scientific Research at King Saud University.

Acknowledgments: The authors would like to acknowledge the College of Engineering Research Center at King Saud University in Riyadh for their financial support in carrying out the research reported in this paper. The authors also thank the Deanship of Scientific Research at King Saud University for their technical support.

Conflicts of Interest: The authors declare no conflict of interest.

References

1. Cole, C.S.; Sherman, A.M. Lightweight materials for automotive applications. *Mater. Charact.* **1995**, *35*, 3–9. [CrossRef]
2. Miller, W.S.; Zhuang, L.; Bottema, J.; Wittebrood, A.; de Smet, P.; Haszler, A.; Vieregge, A.J.M.S. Recent development in aluminum alloys for the automotive industry. *Mater. Sci. Eng. A* **2000**, *280*, 37–49. [CrossRef]
3. Goehler, D.D. *Procedings of Innovations and Advancements in Aluminum Casting Technology—AFS Special Conference, City of Industry, CA, 1988*; American Foundarymen's Society: Des Plaines, IL, USA, 1998; pp. 103–106.
4. Palazzo, F. The future of aluminum in the automotive industry. *Aluminio* **1977**, *46*, 323–334.
5. Frid lyander, I.N. Aluminum alloys in aircraft in the periods of 1970–2000 and 2001–2015. *Met. Sci. Heat Treat.* **2001**, *43*, 6–10. [CrossRef]
6. Spada, A.T. Search of lightweight components: Automotive cast aluminum conversion. *Eng. Cast. Solut.* **2002**, *4*, 28–31.
7. Hosford, W.F.; Fleischer, R.L.; Backofen, W.A. Tensile deformation of aluminium single crystals. *Acta Met.* **1960**, *8*, 187–199. [CrossRef]
8. Dumoulin, S.; Tabourot, L. Experimental data on aluminium single crystals behaviour. *Proc. IMechE Part C J. Mech. Eng. Sci.* **2005**, *219*, 1159.
9. Moszczyńska, D.; Adamczyk-Cieślak, B.; Osiak, B.; Lipiec, R.; Kulczyk, M.; Mizera, J. Microstructure and texture development in a polycrystal and different aluminium single crystals subjected to hydrostatic extrusion. *Bull. Mater. Sci.* **2019**, *42*, 110. [CrossRef]
10. Filippov, P.; Koch, U. Nanoindentation of aluminum single crystals: Experimental study on influencing factors. *Materials* **2019**, *12*, 3688. [CrossRef]
11. Kaufman, J.G.; Rooy, E.L. *Aluminum Alloy Castings: Properties, Processes, and Applications*; ASM International, Materials Park: Novelty, OH, USA, 2004.
12. Yang, C.; Zhu, K.; Liu, Y.; Cai, Y.; Liu, W.; Zhang, K.; Huang, J. A comparative study of fatigue energy dissipation of additive manufactured and cast $AlSi_{10}Mg$ alloy. *Metals* **2021**, *11*, 1274. [CrossRef]
13. So, H.; Won, S.; Park, J.; Ju Oh, S.; Kang, L.; Kim, K. Mechanical properties and microstructural evolution in Al–Cu–Mg–Ag alloy with a $Cu_xMg_{x/10}$ content. *Mater. Sci. Eng. A* **2021**, *824*, 141573. [CrossRef]
14. Huda, Z.; Taib, N.; Zaharinie, T. Characterization of 2024-T3: An aerospace aluminum alloy. *Mater. Chem. Phys.* **2009**, *113*, 515–517. [CrossRef]
15. Wang, Q.G. Microstructural effects on the tensile and fracture behavior of aluminum casting alloys A356/357. *Metall. Mater. Trans. A* **2003**, *34*, 2887–2899. [CrossRef]
16. Gazizov, M.; Kaibyshev, R. Precipitation structure and strengthening mechanisms in an Al-Cu-Mg-Ag alloy. *Mater. Sci. Eng. A* **2017**, *702*, 29–40. [CrossRef]
17. Gupta, A.K.; Gaunt, P.; Chaturvedi, M.C. The crystallography and morphology of the S′-phase precipitate in an Al(CuMg) alloy. *Philos. Mag. A* **1987**, *55*, 375–387. [CrossRef]
18. Alshammari, T.T.; Alharbi, H.F.; Soliman, M.S.; Ijaz, M.F. Effects of Mg content on the microstructural and mechanical properties of Al-4Cu-xMg-0.3Ag alloys. *Crystals* **2020**, *10*, 895. [CrossRef]
19. Abdo, H.S.; Seikh, A.H.; Muhammad, J.A.; Soliman, M.S. Alloying elements effects on electrical conductivity and mechanical properties of newly fabricated Al based alloys produced by conventional casting process. *Materials* **2021**, *14*, 3971. [CrossRef]
20. Zheng, Y.; Xiao, W.L.; Ge, S.J.; Zhao, W.T.; Hanada, S.; Ma, C.L. Effects of Cu content and Cu/Mg ratio on the microstructure and mechanical properties of Al-Si-Cu-Mg alloys. *J. Alloys Compd.* **2015**, *649*, 291–296. [CrossRef]
21. Bakavos, D.; Prangnell, P.B.; Bes, B.; Eberl, F. The effect of silver on microstructuralevolution in two 2xxx series Al-alloys with a high Cu:Mg ratio during ageing to a T8 temper. *Mater. Sci. Eng.* **2008**, *A491*, 214–223. [CrossRef]
22. Gable, B.M.; Shiflet, G.J.; Starke, E.A. Alloy development for the enhanced stabilityof Ω precipitates in Al-Cu-Mg-Ag alloys. *Metall. Mater. Trans.* **2006**, *37*, 1091–1105. [CrossRef]

23. Ringer, S.P.; Yeung, W.; Muddle, B.C.; Polmear, I.J. Precipitate stability in Al-Cu-MgAg alloys aged at high temperatures. *Acta Metall. Mater.* **1994**, *42*, 1715–1725. [CrossRef]
24. Reich, L.; Murayama, M.; Hono, K. Evolution of Ω phase in an Al-Cu-Mg-Ag alloy-Athree-dimensional atom probe study. *Acta Mater.* **1998**, *46*, 6053–6062. [CrossRef]
25. Hutchinson, C.R.; Fan, X.; Penyciik, S.J.; Shiflet, G.J. On the origin of the high coarsening resistance of Ω plates in Al-Cu-Mg-Ag alloys. *Acta Mater.* **2001**, *49*, 2827. [CrossRef]
26. Taylor, J.A.; Parker, B.A.; Polmear, I.J. Precipitation in AI-Cu-Mg-Ag casting alloy. *Met. Sci.* **1978**, *12*, 478–482. [CrossRef]
27. Teixeira, J.D.; Cram, D.G.; Bourgeois, L.; Bastow, T.J.; Hill, A.J.; Hutchinson, C.R. On the strengthening response of aluminum alloys containing shear-resistant plate shaped precipitates. *Acta Mater.* **2008**, *56*, 6109–6122. [CrossRef]
28. Molina, R.; Amalberto, P.; Rosso, M. Mechanical characterization of aluminium alloys for high temperature applications. Part1: Al-Si-Cu alloys. *Metall. Sci. Technol.* **2011**, *29*, 5–15.
29. Xiao, D.H.; Wang, J.N.; Ding, D.Y.; Yang, H.L. Effect of rare earth Ce addition on the microstructure and mechanical properties of an Al–Cu–Mg–Ag alloy. *J. Alloy. Compd.* **2003**, *352*, 84–88. [CrossRef]
30. Shyam, A.; Roy, S.; Shin, D.; Poplawsky, J.D.; Allard, L.F.; Yamamoto, Y.; Morris, J.R.; Mazumder, B.; Idrobo, J.C.; Rodriguez, A.; et al. Elevated temperature microstructural stability in cast AlCuMnZr alloys through solute segregation. *Mater. Sci. Eng.* **2019**, *A765*, 138279. [CrossRef]
31. Gao, Y.H.; Yang, C.; Zhang, J.Y.; Cao, L.F.; Liu, G.; Sun, J.; Ma, E. Stabilizing nano precipitates in Al-Cu alloys for creep resistance at 300 degrees C. *Mater. Res. Lett.* **2019**, *7*, 18–25. [CrossRef]
32. Zhao, Q.; Liu, Z.; Huang, T.; Xia, P.; Li, F. Enhanced fracture toughness in an annealed Al-Cu-Mg alloy by increasing Goss/Brass texture ratio. *Mater. Charact.* **2016**, *119*, 47–54. [CrossRef]
33. Wang, X.; Guo, M.; Cao, L.; Luo, J.; Zhang, J.; Zhuang, L. Effect of heating rate on mechanical property, microstructure and texture evolution of Al-Mg-Si-Cu alloy during solution treatment. *Mater. Sci. Eng. A* **2015**, *621*, 8–17. [CrossRef]
34. Buken, H.; Kozeschnik, E. Modeling static recrystallization in Al-Mg Alloys. *Metall. Mater. Trans. A* **2021**, *52*, 544–552. [CrossRef]
35. Mei, Z.; Liu, Z.; Bai, S.; Wang, J.; Cao, J. Effects of Yatrium addittions on microstructure and mechanical properties of cast Al-Cu-Mg alloys. *J. Alloys Compd.* **2021**, *870*, 159435. [CrossRef]
36. Xie, H.; Zhao, J.; Cao, J.; Luo, L.; Guo, S.; Ou, L.; Liu, Z.; Bai, S. Effects of minor Er addittions on the microstructure and mechanical properties of cast Al-Cu-Mg-Ag alloys. *Materials* **2021**, *14*, 4212. [CrossRef] [PubMed]
37. Wang, J.; Liu, Z.; Bai, S.; Cao, J.; Zhao, J.; Luo, L.; Li, J. Microstructure evolution and mechanical properties of the electron-beam welded joints of cast Al-Cu-Mg-Ag alloy. *Mater. Sci. Eng.* **2021**, *A801*, 140363. [CrossRef]
38. Tiryakioglu, M.; Campbell, J. Ductility, structural quality, and fracture toughnessof Al-Cu-Mg-Ag (A201) alloy castings. *Mater. Sci. Technol.* **2009**, *25*, 784–789. [CrossRef]
39. Rakhmonov, J.; Liu, K.; Pan, L.; Breton, F.; Chen, X.G. Enhanced mechanical properties of high-temperature-resistant Al-Cu cast alloy by microalloying with Mg. *J. Alloy. Compd.* **2020**, *827*, 154305. [CrossRef]
40. Zamani, M.; Toschi, S.; Morri, A.; Ceschini, L.; Seifeddine, S. Optimisation of heat treatment of Al-Cu-(Mg-Ag) cast alloys. *J. Therm. Anal. Calorim.* **2020**, *139*, 3427–3440. [CrossRef]
41. Feng Li, J.; Ziqiao, Z.; Na, J.; Chengyu, T. Localized corrosion mechanism of 2×××-series Al alloy containing S(Al_2CuMg) and θ (Al_2Cu) precipitates in 4.0% NaCl solution at pH 6.1. *Mater. Chem. Phys.* **2005**, *91*, 325–329.
42. Liu, Q.; Zhu, R.; Li, J.; Chen, Y.; Zhang, X.; Zhang, L.; Zheng, Z. Microstructure evolution of Mg, Ag and Zn micro-alloyed Al-Cu-Li alloy during homogenization. *Trans. Nonferrous Met. Soc. China* **2016**, *26*, 607–619. [CrossRef]
43. García-Hernández, J.L.; Garay-Reyes, C.G.; Gómez-Barraza, I.K.; Ruiz-Esparza-Rodríguez, M.A.; Gutiérrez-Castañeda, E.J.; Estrada-Guel, I.; Maldonado-Orozco, M.C.; Martínez-Sánchez, R. Influence of plastic deformation and Cu/Mg ratio on the strengthening mechanisms and precipitation behavior of AA2024 aluminum alloys. *J. Mater. Res. Technol.* **2019**, *8*, 5471. [CrossRef]
44. Deschamps, A.; Bastow, T.J.; de Geuser, F.; Hill, A.J.; Hutchinson, C.R. In situ evaluation of the microstructure evolution during rapid hardening of an Al-2.5Cu-1.5Mg (wt.%) alloy. *Acta Mater.* **2011**, *59*, 2918–2927. [CrossRef]
45. Basu, I.; Pradeep, K.G.; Mieβen, C.; Barrales-Mora, L.A.; Al-Samman, T. The role of atomic scale segregation in designing highly ductile magnesium alloys. *Acta Mater.* **2016**, *116*, 77–94. [CrossRef]
46. Gladman, T. On the theory of the effect of precipitate particles on grain growth in metals. *Proc. R. Soc. Lond. A* **1966**, *294*, 298–309.
47. Humphreys, F.J. A unified theory of recovery recrystallization and grain growth, based on the stability and growth of cellular microstructures-II. The effect of second-phase particles. *Acta Mater.* **1977**, *45*, 5031–5039. [CrossRef]
48. Humphreys, F.J.; Hatherly, M. *Recrystallization and Related Annealing Phenomena*; Pergamon: Oxford, UK; Elsevier: Amsterdan, The Netherlands, 2004.
49. Koch, C.C.; Ovid'ko, I.A.; Seal, S.; Veprek, S. *Structural Nanocrystalline Materials: Fundamentals and Applications*; Cambridge University Press: Cambridge, UK, 2007.
50. Nes, E.; Ryum, N.; Hunderi, O. On the zener drag. *Acta Metall.* **1985**, *33*, 11–22. [CrossRef]
51. Takata, N.; Yoshida, F.; Ikeda, K.; Nikashima, H.; Abe, H. Abnormal grain growth of off-cube grains in high purity aluminum foils with cube texture. *Mater. Trans.* **2005**, *46*, 2975–2980. [CrossRef]
52. Xu, Y.; Naguami, H.; Han, Y.; Zhang, G.; Zhai, T. The deformation behavior and microstructure evolution of a Mn- and Cr-containing Al-Mg-Si-Cu alloy during hot compression and subsequent heat treatment. *Metall. Mater. Trans. A* **2017**, *48*, 1355–1365. [CrossRef]

53. Dennis, J.; Bate, P.S.; Humphreys, F.J. Abnormal grain growth in Al-3.5Cu. *Acta Mater.* **2009**, *57*, 4539–4547. [CrossRef]
54. Sztwiertnia, K.; Bieda, M.; Korneva, A. Continuous and discontinuous recrystallization of 6013 aluminum alloy. *Mater. Sci. Forum* **2013**, *753*, 221–224. [CrossRef]
55. Uttarasak, K.; Chongchitnan, W.; Matsuda, K.; Chairuangsri, T.; Kajornchaiyakul, J.; Banjongprasert, C. Evolution of fe-containing intermetallic phases and abnormal grain growth in 6063 aluminum alloy during homogenization. *Results Phys.* **2019**, *15*, 102535. [CrossRef]
56. King, S.J.; Kim, Y.; Kim, M.; Zuo, J. Determination of interfacial atomic structure, misfits and energetics of Ω phase in Al–Cu–Mg–Ag alloy. *Acta Mater.* **2014**, *81*, 501–511. [CrossRef]
57. Ryen, Ø.; Holmedal, B.; Nijs, O.; Nes, E.; Sjölander, E.; Ekström, H.E. Strengthening mechanisms in solid solution aluminum alloys. *Metall. Mater. Trans. A* **2006**, *37*, 1999. [CrossRef]